Journal of Hazardous Materials 219–220 (2012) 133–140

Contents lists available at SciVerse ScienceDirect

Journal of Hazardous Materials

journal homepage: www.elsevier.com/locate/jhazmat

Quasi-Monte Carlo based global uncertainty and sensitivity analysis in modeling free product migration and recovery from petroleum-contaminated aquifers

Li He[a,*], Gordon Huang[b], Hongwei Lu[b], Shuo Wang[a], Yi Xu[b]

[a] MOE Key Laboratory of Regional Energy and Environmental Systems Optimization, Resources and Environmental Research Academy, North China Electric Power University, Beijing 102206, China
[b] Chinese Academy for Environmental Planning, Beijing 100012, China

ARTICLE INFO

Article history:
Received 1 October 2011
Received in revised form 17 March 2012
Accepted 26 March 2012
Available online 3 April 2012

Keywords:
Global uncertainty and sensitivity analysis
GLUE
Quasi-Monte Carlo
Free product recovery
Aquifer remediation

ABSTRACT

This paper presents a global uncertainty and sensitivity analysis (GUSA) framework based on global sensitivity analysis (GSA) and generalized likelihood uncertainty estimation (GLUE) methods. Quasi-Monte Carlo (QMC) is employed by GUSA to obtain realizations of uncertain parameters, which are then input to the simulation model for analysis. Compared to GLUE, GUSA can not only evaluate global sensitivity and uncertainty of modeling parameter sets, but also quantify the uncertainty in modeling prediction sets. Moreover, GUSA's another advantage lies in alleviation of computational effort, since those globally-insensitive parameters can be identified and removed from the uncertain-parameter set. GUSA is applied to a practical petroleum-contaminated site in Canada to investigate free product migration and recovery processes under aquifer remediation operations. Results from global sensitivity analysis show that (1) initial free product thickness has the most significant impact on total recovery volume but least impact on residual free product thickness and recovery rate; (2) total recovery volume and recovery rate are sensitive to residual LNAPL phase saturations and soil porosity. Results from uncertainty predictions reveal that the residual thickness would remain high and almost unchanged after about half-year of skimmer-well scheme; the rather high residual thickness (0.73–1.56 m 20 years later) indicates that natural attenuation would not be suitable for the remediation. The largest total recovery volume would be from water pumping, followed by vacuum pumping, and then skimmer. The recovery rates of the three schemes would rapidly decrease after 2 years (less than 0.05 m^3/day), thus short-term remediation is not suggested.

1. Introduction

Nonaqueous phase liquids (NAPLs) are among the most common type of pollutants in soils and groundwater. Their presence can create a hazard to public health and the environment. One of the widely-encountered sources of NAPLs is the spills involving the release of petroleum products such as gasoline, diesel fuel and lubricating and heating oil from underground leaking oil tanks and pipelines. Light NAPLs (LNAPLs), existing as a type of free product in the subsurface, can be recovered through skimmer (i.e., no pumping is implemented), water pumping and vacuum pumping schemes [1–3]. Free product recovery has increasingly received attention in the past years due to its economic and temporal efficiencies [3,4].

Studies have been conducted in modeling migration and recovery of free product (LNAPLs) in unconfined aquifers [3,5,6]. Kaluarachchi and Parker [1] developed a numerical model named ARMOS to simulate free product migration and recovery in unconfined aquifers. Based on the assumption of local vertical equilibrium, the area flow equations for water and hydrocarbon can be derived with reduced dimensionality and nonlinearity. The model was also capable of simulating free phase hydrocarbons under conditions involving hydrocarbon skimming with or without water pumping. Kaluarachchi [3] investigated the effects of subsurface heterogeneity on free-product recovery system designs using a vertically integrated three-phase flow model. Results from a series of hypothetical field-case simulation revealed that the effects were enhanced at relatively low water-pumping rates, and the difference in results produced by homogeneous and heterogeneous simulations was substantial.

Charbeneau et al. [7] proposed two simple models for predicting free product recovery rates using wells and vacuum pumping systems. The models incorporated vertical variations in LNAPL saturation and relative permeability through the use of effective LNAPL-layer values. Compared to ARMOS, the models were rather simple but their applicability was unable to address multiple-well pumping strategies. Li et al. [8] presented the simulation of a dual-phase vacuum extraction process via a finite element multiphase flow model. It was observed that the model was computationally

* Corresponding author. Tel.: +86 10 61772980; fax: +86 10 61772960.
E-mail address: heliy111@gmail.com (L. He).

0304-3894/$ – see front matter © 2012 Elsevier B.V. All rights reserved.
http://dx.doi.org/10.1016/j.jhazmat.2012.03.067

efficient due to the vertical integration of governing equations for water, oil, and gas flow. Yen and Chang [9] used a bioslurping simulation model for predicting three-phase (water, oil, and gas) flow and transport in groundwater and gas phase flow in the unsaturated zone. Through the model, one can gain insight into the recovery and migration of LNAPLs with vacuum enhanced recovery and multispecies (dissolved in groundwater) and gas phases (in unsaturated zone) transport in heterogeneous, anisotropic porous media.

The above mentioned efforts in free product recovery were presented as either analytical equations or two-dimensional numerical models. However, few of the studies considered the impacts of parameter uncertainty on LNAPL migration and recovery processes [3]. Due to inevitable errors in modeling formulation, data observation and parameter estimations, model predictions could depart from the true values considerably [10–15]. Sensitivity analysis is an effective approach for analyzing effects of parameter variations on remediation performance. However, it investigates the impacts by treating the parameters as individual values rather than sets of values [16]. Recently, generalized likelihood uncertainty estimation (GLUE) methods have been widely applied in for calibration and uncertainty estimation of mathematical models [16–26].

However, GLUE does not consider individual or interactive influences of parameters on predictions. This probably leads to the increase in computational effort since overmuch uncertain parameters need to be considered by GLUE. If global sensitivity analysis (GSA) is performed before GLUE, then those substantially sensitive parameters can be screened out and input to GLUE procedures. Due to the decrease of uncertainty parameters, the required realizations can be reduced. Moreover, GLUE generally employs regular Monte Carlo (MC) sampling with an assumption of uniformly-distributed random parameters, while MC cannot guarantee the sampling data are generated with low discrepancy. This causes slow convergence rate in computation and probably in underestimation of uncertainty predictions due to high possibility of missing part of important parameter values in sampling. Much research has been undertaken in development and application of high-efficient sampling rules such as Latin Hypercube (LH), Markov Chain Monte Carlo (MCMC), adaptive MCMC [26], and quasi-Monte Carlo (QMC). Particularly, QMC has shown its superior advantages over regular MC in generating low-frequency sampling data and high efficiency over LH [27].

Therefore, this paper aims to present a new global uncertainty and sensitivity analysis (GUSA) framework based on GSA and GLUE methods. Through GUSA, not only global sensitivity and uncertainty of input parameters can be evaluated, but also uncertainty in modeling predictions can be quantified. GUSA is applied to a practical petroleum-contaminated site in Canada to investigate free product migration and recovery processes under aquifer remediation schemes.

2. Materials and methods

2.1. Aquifer overview

The aquifer to be investigated is located at the Cantuar site in southwest Saskatchewan, Canada [33]. The existing site characterization results showed that the stratigraphy at the aquifer consisted of native silt and silty clay extending from surface to between approximately 7.6 m and 12.5 m depth. Underlying silty clay was clay matrix till extending to between 9.4 m and 15.2 m depth. Sand was encountered with or underlying the clay matrix till between approximately 9.4 m and 15.2 m depth. Silty clay and sand underlying the top soil were over majority of the aquifer. Clay/till underlay the sand over the majority of the site, and extended to the maximum exploration depth of 14.0 m. Groundwater table was measured between approximately 4.8 m and 13.2 m below ground surface, predominantly located in the clay tills. The groundwater flow direction was from southeast toward northwest with a gradient of approximately 0.1 m/m.

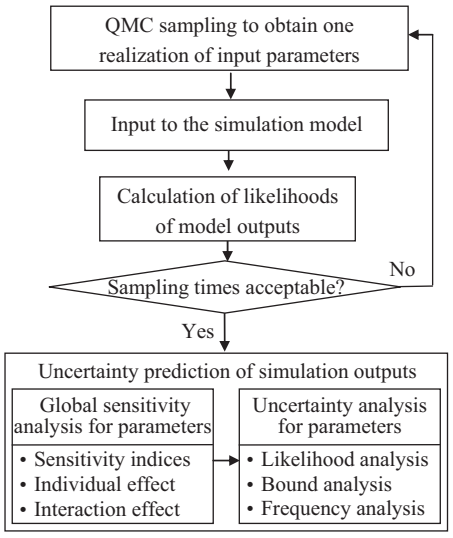

Fig. 1. Flowchart of QMC-based GUSA.

Free phase hydrocarbons (i.e., free product) have infiltrated through fractures near an underground storage tank ever buried into the subsurface. The hydrocarbons migrated along saturated fissures in the clay vertically toward the groundwater table, and finally piled up at the groundwater surface. Fig. S3 in the Supplementary data shows the monitoring well locations and estimated contamination plume of the aquifer. During the 25-April-2000 monitoring program, free product was detected in monitoring wells BH101 (725 mm), BH103 (1773 mm), BH105 (545 mm), BH106 (201 mm), BH108 (176 mm), BH110 (398 mm), BH111 (250 mm), BH201 (453 mm), BH202 (192 mm) and BH401 (262 mm) located across the site. Fig. S4 in the Supplementary data presents the free product thickness on 25th May, 2000 at the site, which indicated that the peak free phase hydrocarbon thickness was approximately in the range of 1.8–2.5 m. The GUSA framework was applied to this aquifer to evaluate performance of three potential aquifer remediation schemes. Note that this section, only residual free product thickness, total recovery volume and recovery rate were examined at well BH401 under three 20-year remediation schemes: skimmer, water pumping (1 m^3/hr), and vacuum pumping (−4 m water column).

2.2. Global uncertainty and sensitivity analysis

The QMC-based GUSA framework is shown in Fig. 1. In terms of the figure, a mathematical simulation model is selected for capturing the free product migration and recovery processes in an unconfined aquifer. The model can be used to predict the free product migration and recovery processes under pumping-based remediation schemes. The following gives the volume balance equations for water, NAPL and air phases in the unsaturated and saturated zones [2,3,28]:

$$\frac{\partial V_w}{\partial t} = \frac{\partial}{\partial x_i}\left(T_{wij}\frac{\partial Z_{aw}}{\partial x_j}\right) + R_w\delta(x_i - x_i^*)\delta(x_j - x_j^*) \quad (1)$$

$$\frac{\partial V_o}{\partial t} = \frac{\partial}{\partial x_i}\left(T_{oij}\frac{\partial Z_{ao}}{\partial x_j}\right) + R_o\delta(x_i - x_i^*)\delta(x_j - x_j^*) \quad (2)$$

$$\frac{\partial V_a}{\partial t} = \frac{\partial}{\partial x_i}\left(T_{aij}\frac{\partial Z_{aa}}{\partial x_j}\right) + R_a\delta(x_i - x_i^*)\delta(x_j - x_j^*) \quad (3)$$

where V_w, V_o, and V_a are specific volume of water, NAPL, and gas, respectively [L]; T_{wij}, T_{oij}, and T_{aij} are transmissivity of water, NAPL, and gas, respectively [$L^2\,T^{-1}$]; Z_{aw} is air-water table elevation [L], where water pressure is zero; Z_{ao} is air-NAPL table elevation [L], where NAPL pressure is zero; Z_{aa} is gas pressure [L]; R_w, R_o, and R_a are pumping rates of water, NAPL, and gas, respectively [$L^3\,L^{-2}\,T^{-1}$]; δ is the Dirac delta function; x_i and x_j are Cartesian coordinates, representing the horizontal and lateral direction, respectively; (x_i^*, x_j^*) is the location of the pumping well; t is time [T]. The specific volume of water, NAPL, and gas can be expressed as follows:

$$V_w = \int_{Z_L}^{Z_u} \phi S_w dz \quad (4)$$

$$V_o = \int_{Z_L}^{Z_u} \phi S_o dz \quad (5)$$

$$V_a = \int_{P_{ao}}^{Z_s} \phi S_a dz \quad (6)$$

$$T_{wij} = \int_{Z_L}^{Z_u} k_{rw}K_{swij} dz \quad (7)$$

$$T_{oij} = \int_{Z_L}^{Z_u} k_{ow}K_{soij} dz \quad (8)$$

$$T_{aij} = \int_{P_{ao}}^{Z_s} k_{ra}K_{saij} dz \quad (9)$$

$$K_{soij} = \frac{\rho_{ro}K_{swij}}{n_{ro}} \quad (10)$$

$$K_{saij} = \frac{\rho_{ra}K_{swij}}{n_{ra}} \quad (11)$$

where ϕ is porosity; k_{rw}, k_{sw}, and k_{sw} are relative permeability of phase water, NAPL, and air, respectively; K_{swij}, K_{soij}, and K_{saij} are saturated hydraulic conductivity tensor of phase water, NAPL, and air, respectively [$L\,T^{-1}$]; ρ_{ro} and ρ_{ra} are specific gravity of NAPL and air phase, respectively; n_{ro} is ratio of NAPL to water dynamic viscosity; n_{ra} is ratio of air to water dynamic viscosity; Z_u and Z_L are upper and lower limits of integration for water and NAPL phases [L], respectively; Z_s is ground surface elevation [L]; P_{ao} is elevation of air-NAPL interface [L]; z is vertical coordinate [L]; S_w, S_o, and S_a are water, NAPL, and air phase saturation, respectively, which can be solved by [1,28]:

$$\frac{\partial(\phi S_w\rho_w)}{\partial t} = \frac{\partial[\rho_w k_{rw}K_{swij}(\partial h_w/\partial x_j + \rho_{rw}u_j)]}{\partial x_i} \quad (12)$$

$$\frac{\partial(\phi S_o\rho_o)}{\partial t} = \frac{\partial[\rho_o k_{ro}K_{soij}(\partial h_o/\partial x_j + \rho_{ro}u_j)]}{\partial x_i} \quad (13)$$

$$\frac{\partial(\phi S_a\rho_a)}{\partial t} = \frac{\partial[\rho_a k_{ra}K_{saij}(\partial h_a/\partial x_j + \rho_{ra}u_j)]}{\partial x_i} \quad (14)$$

$$S_w + S_o + S_a = 1 \quad (15)$$

where h_w, h_o, and h_a are density of water, NAPL and air phase, respectively [L]; ρ_{rw} is specific gravity of water; ρ_w, ρ_o, and ρ_a are density of water, NAPL and air phase, respectively [$M\,L^{-3}$]; u_j is unit gravitational vector measured positive upwards ($u_j = \partial z/\partial x_j$, where z is elevation). In addition to equations (1)–(15), many other constitutive equations, initial conditions and boundary conditions should be identified. More details regarding the modeling formulation and solution are shown in Fig. S1 and Section S1 in the Supplementary data. Output variables from the above equations include specific volume, saturation and thickness of the water, NAPL, and gas phases.

Considering the uncertainty in parameters (either stochastic- or interval-valued), QMC sampling technique can be employed to obtain a number of realizations of uncertain parameter sets, with each one comprised of all uncertain parameters whose global sensitivities need to be examined. Each of the realizations of parameter sets can then be input to the simulation model for computing one realization of prediction sets (a set is comprised of all output variables). Different from regular MC and LH sampling rules, QMC is capable of avoiding obtaining unevenly-distributed parameters within the sampling space. It has shown its efficiency in randomly sampling as it is based on low-discrepancy sequences, which is different from regular MC method based on sequences of pseudorandom parameters. QMC and MC can be described in a similar way; however, QMC generates a subsequence of random samples (i.e., realizations of random parameters) with low discrepancy to replace uniformly distributed random parameters [14,29]. Discrepancy measures the extent to which the samples are evenly dispersed in an s-dimensional unit hypercube, I^s (defined as $I^s = [0,1] \times \ldots \times [0,1]$). Here dimensionality represents the number of potentially-sensitive parameters to be examined by QMC. If assuming to generate a set of samples $(x_1, \ldots, x_N)$ from the unit hypercube, then the discrepancy of samples $x_1, \ldots, x_N$ can be defined as:

$$D_N = \sup_{R\in[0,1]^s}\left|\frac{\text{number of points in } R}{N} - V(R)\right| \quad (16)$$

where R represents all subsets of the s-dimensional unit hypercube; $V(R)$ is the volume of R. Note that D_N has the property of

$$\lim_{N\to\infty} D_N = 0 \quad (17)$$

which means that when the sampling times is large enough, the discrepancy will approximate to zero, thus generating the most evenly-distributed parameter realizations. Since MC has no such property, it is obvious that the accuracy of QMC increases faster than MC with the growth of sampling times. The accuracy of QMC can be defined based on the Koksma-Hlawka inequality for approximation error [14]:

$$D_N \le D_{N0} = K\frac{(\ln N)^s}{N} \quad (18)$$

where K is a constant dependent of the sequence but independent of N. If $D_N \le D_{N0}$, then accept the sample; otherwise, discard it.

GSA can be performed in terms of sensitivity indices (say, Sobol indices) computed via QMC. Generally, the higher an index value, the more significant impact it will have on predictions. Sensitivity indices can be classified as individual index (considering one parameter), interaction index (considering multiple parameters) and total individual index (considering one parameter and its interactions with all other parameters) [30]. For example, assume the individual (or 1st-order) sensitivity indices for 3 parameters to be S_1, S_2, and S_3. Then the 2nd-order interaction sensitivity indices are S_{12}, S_{13}, S_{23}, and the 3rd-order index is S_{123}. The total individual sensitivity index can be defined as $ST_i = S_i + S_{ij} + S_{ijk}$ ($i = 1, 2, 3$; $i \ne j \ne k$). The specific algorithm for computing Sobol indices via QCM is detailed in Section S2 of the Supplementary data. By comparing the values of sensitivity indices, those parameters with significant impacts can be screened out and then introduced to the GLUE method for uncertainty estimations.

With the screened-out sensitive parameters, uncertainty analysis is conducted using the GLUE method [17]. In this step, likelihood function values, realizations frequency and bounded values can be good criteria to gain insight into properties of uncertain parameters. GLUE assumes that there is more than one "optimal"

model structure or parameter set that can be found to capture an input–output relationship [19]. Based on generalized likelihood measures, GLUE accepts those models (including parameter estimates) with behavioral simulations based on which the calculated likelihood is greater than a tolerable value. In comparison, those models assumed to be unacceptable or non-behavioral may be rejected by being given a likelihood of zero.

Five requirements should be satisfied by GLUE [19]. The first is determination of a candidate model that will be used to capture the relationship between predictor variables and response variables. Multiple candidate models can also be used if they have identical uncertain parameters and can be evaluated in the same way. The second is collection of a series of observed data, which need to be compared with simulated results and further used for calculation of likelihood values. The third is definition of an appropriate likelihood measure for judging the quality of the model. Such a measure should consider the variability of the observed data and reflect the closeness of simulated and observed results. In addition, a critical value of likelihood should be given before running GLUE. For each of the candidate model (including the chosen parameters), the likelihood is calculated based on the simulated and observed results and then compared with the critical value. If it is larger than the critical value, the model is accepted; otherwise, the model is rejected. During the past years, a number of likelihood measures have been used including U-uncertainty measure [31], Nash and Sutcliffe efficiency coefficient [16,18,19], Shannon entropy measure H- and U-uncertainty measures [20], Whittle's likelihood [16], etc. Note that selection of a likelihood measure and its critical value depends on the subjective choice of model users. In this study, the likelihood function is defined as [18]:

$$L(\hat{\theta}|Y_1^O, Y_2^O, \cdots Y_m^O) = \begin{cases} \dfrac{R^2}{R^2_{\max}} & 0 \le R^2 \le 1 \\ 0 \quad \text{otherwise} \end{cases} \tag{19}$$

$$R = 1 - \frac{\sum_{i=1}^{m} (Y_i^O - Y_i^S)^2}{\sum_{i=1}^{m} (Y_i^O - \bar{Y}^O)^2} \tag{20}$$

where L is likelihood function; $\hat{\theta}$ is vector of estimated parameters; Y_i^O and Y_i^S are observed and simulated data, respectively; $\bar{Y}^O$ is the mean of the observed data; R^2 is Nash and Sutcliffe efficiency coefficient; $R^2_{\max}$ represents the maximum efficiency value found within the set of model realizations; m is the number of observed data.

The fourth is identification of the sampling range of each uncertain parameter, varying from its lower to upper bound. This is not difficult in practice as the ranges can be determined from various references, public survey, or monitoring results. However, the range should neither be too large (to avoid increasing computational effort) nor too small (to avoid missing some important information). The last is selection of a sampling technique to obtain potential realizations of uncertain parameters. QMC sampling is also used to replace conventional MC for accelerating convergence rate [19].

Uncertainty prediction is performed in the last step to understand statistical properties of simulation outputs, including lower bound, upper bound, mean value, possibility, and even probability distribution [18]. It is obvious that the proposed GUSA can be regarded as an improvement of existing GLUE methods. Through GUSA, not only global sensitivity and uncertainty of modeling parameters can be evaluated, but also uncertainty in modeling predictions can be quantified. Compared to GLUE, GUSA's major advantage lies in alleviation of computational effort, since those globally-insensitive parameters can be identified and removed from the uncertain-parameter set.

3. Results

To begin, a group of two-dimensional scatter plots are shown in Fig. S2 in the Supplementary data to compare the difference in three sampling rules: MC, LHS, and QMC. The QMC sampling rule was programmed in Fortran 77 using the Halton sequence [32]. Discrepancies were computed according to equation [21] for comparison. It is found that discrepancies obtained from MC, LH, and QMC are 0.042, 0.052, and 0.022, respectively, when 100 samples are obtained; these values respectively decrease to 0.023, 0.026 and 0.018 for 400 sampling times and to 0.015, 0.017, and 0.008 for 900 sampling times. Thus, on the one hand, the discrepancies can rise with increasing sampling times whatever sampling techniques are used. On the other hand, QMC generates the lowest discrepancy values, followed by MC and then LH; this is similar to the conclusion from Pan and Thompson [27].

The previous work regarding this site revealed that soil porosity and residual LNAPL saturations (in unsaturated and saturated zones) could have impacts on predictions. This guess was tested through GSA based on Sobol indices. Table S1 in the Supplementary data lists estimated interval ranges of the four parameters (i.e., soil porosity, residual NAPL saturation in the unsaturated zone, residual NAPL saturation in the saturated zone, and initial free product thickness) and part of deterministic parameters. According to Sobol [30], assume 10,000 samples representing realizations of input parameters were divided into 5000 groups, with each one containing 2 samples. Assume one group to be (P_{1i}, P_{2i}, P_{3i} and P_{4i}) and the other one to be (P_{1i}', P_{2i}', P_{3i}' and P_{4i}'), where P_1 to P_4 represent the four uncertain parameters and superscript i is from 1 to 5000. If S_1 and ST_1 need to be computed, then (P_{1i}, P_{2i}, P_{3i} and P_{4i}), (P_{1i}', P_{2i}, P_{3i} and P_{4i}) and (P_{1i}, P_{2i}', P_{3i}' and P_{4i}') are input to the simulation model for separate computation. Similarly, if S_{12} and ST_{12} are required, then (P_{1i}, P_{2i}, P_{3i} and P_{4i}), (P_{1i}', P_{2i}', P_{3i} and P_{4i}) and (P_{1i}, P_{2i}, P_{3i}' and P_{4i}') are input. Note that only (P_{1i}, P_{2i}, P_{3i} and P_{4i}) and (P_{1i}', P_{2i}', P_{3i}' and P_{4i}') are input to the model for the following computation required by GLUE.

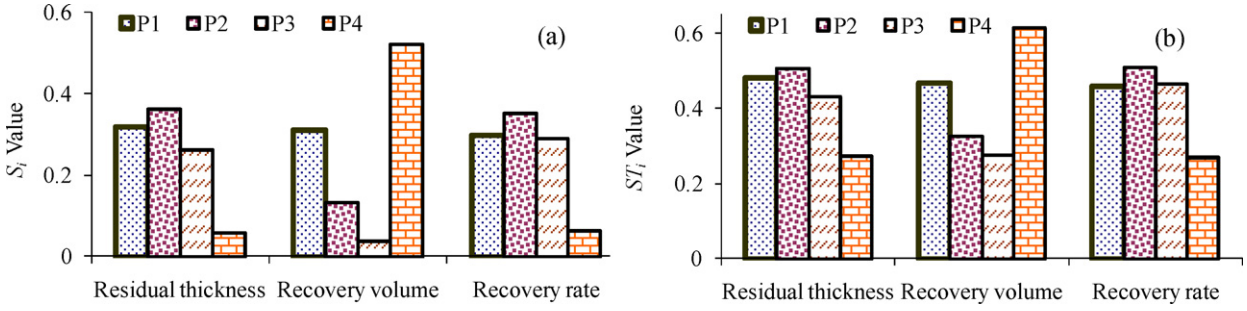

Fig. 2. Sensitivity index values, where S_i and ST_i represent individual and total individual sensitivity index for the ith parameter, respectively; P_1, P_2, P_3 and P_4 represent soil porosity, residual NAPL saturation in the unsaturated zone, residual NAPL saturation in the saturated zone, and initial free product thickness, respectively.

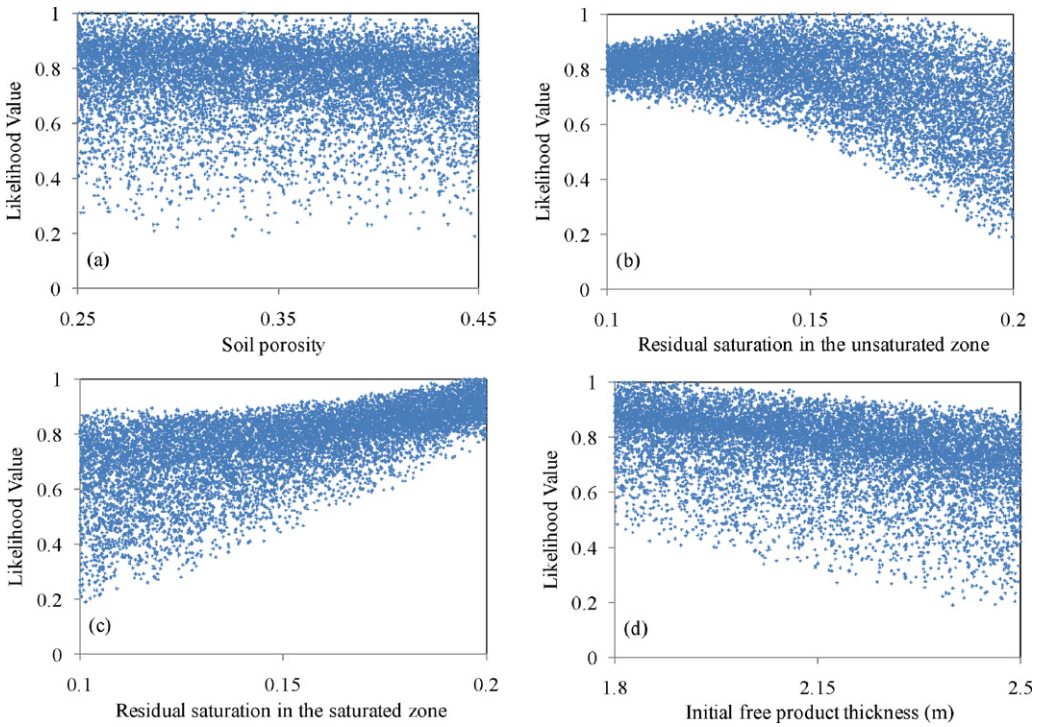

Fig. 3. Likelihood of recovery thickness against four uncertain parameters.

Fig. 2 presents the obtained index values quantifying the individual and total individual effects of parameters (S_i and ST_i) on residual free product thickness, total recovery volume and recovery rate under vacuum pumping. From Fig. 2(a), initial thickness has the most significant impact on total recovery volume (the index value is 0.52). In comparison, recovery thickness and recovery rate are more sensitive to the other three parameters but insensitive to initial thickness. Fig. 2(b) exhibits the total individual effect considering 1st- and 2nd-order impact (i.e., $ST_i = S_i + S_{ij}, i \neq j$). It can be observed that the total individual effect has similar influences on the simulation outputs. This implies that the individual indices can well quantify the global sensitivity of parameters and the interactive effects can thus be ignored.

Since the above evidence showed that the four parameters have influences on simulation outputs, they were represented as interval ranges for further uncertainty analysis. They were not assumed to be stochastic parameters mainly due to lack of sufficient data for statistical inference. It should be mentioned that the observed data only included the total recovery volume from a period of vacuum pumping from 27 April to 14 September (Fig. S5 in the Supplementary data). They were thus used for calibration of the simulation model and computation of the likelihood values for the vacuum pumping scheme. Note that the likelihood values for the other two schemes were not computed due to the lack of monitoring data.

Fig. 3 shows the scatter plots representing the likelihoods of recovery thickness, which were obtained from the 10,000 samples for the vacuum pumping scheme. It is shown that the acceptable values of the parameters can take almost all values falling within their given ranges, with the corresponding likelihoods varying approximately from their lower and upper bounds. It was also found that the likelihoods vary in the range of 0.2–1.0 with soil porosity increasing from 0.25 to 0.45. This indicates that all of the soil porosity levels in the given range could occur in a similar chance (from 0.2 to 1.0). Other implications in the figure are shown as follows. Firstly, a low likelihood means the model is not calibrated well, while a high likelihood indicates the simulated results match well with the observed data. Secondly, a higher-density area indicates a greater possibility of the parameter taking the values within the area. Thirdly, a conventional estimation of individual parameters may not be suitable since many of the acceptable parameter values could have been ignored, while estimation of sets of parameters (even if they are correlated) would better fit the model to observed data; for example, an individual estimate consisted of 0.35 (soil porosity), 0.15 (residual LNAPL saturation in the unsaturated zone), 0.20 (residual LNAPL saturation in the saturated zone) and 2.0 m (initial free product thickness) may not be as good as a set estimate of [0.2, 0.4], [0.10, 0.20], and [0.15, 0.25], and [2.0, 2.2] m (for the four parameters respectively) in fitting observed data. This is why it has been increasingly emphasized the need to treat parameters as sets of values instead of individual values [19].

Histograms can also be obtained from the uncertainty analysis to understand the probability densities of simulation results. Fig. 4 presents the histograms of residual free product thickness and total recovery volume under the vacuum-pumping scheme. The probability densities were derived from the cumulative frequencies of QMC together with GLUE [18]. It is indicated that the residual free product thickness and total recovery volume both follow a non-normal distribution.

Fig. 5 presents the simulation results for the three remediation schemes BH401. Fig. 5(a), (d) and (g) shows the variations of residual free product thickness in the aquifer during 20 years of remediation process. It is apparent that the thickness would remain high and almost unchanged after about half-year skimmer-well pumping; the rather high residual thickness (0.73–1.56 m 20 years later) indicated that natural attenuation would not be suitable for the aquifer remediation. Despite the uncertainty in input parameters, both of the lower- and upper-bounds of residual thickness would decline to less than 0.16 m after 20 years of water- or vacuum-pumping. The water pumping would recover more free products than vacuum pumping, since one would have 95% confidence that the residual thickness would be decreased to a quite low level ([0.01, 0.02] m), while the vacuum pumping would fall to a level of [0.02 to 0.16] m. This suggested the designed vacuum pumping would not be suitable for cleaning up this aquifer since

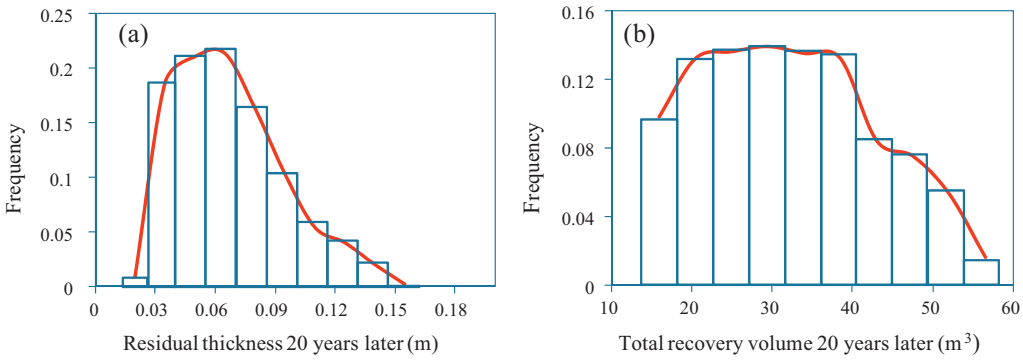

Fig. 4. Histograms indicating probability density of free product thickness and total recovery volume under the vacuum-pumping scheme.

the residual free product (0.16 m in thickness) may pose risk to the aquifer as a permanent contamination source. The 95% CI were calculated by performing statistical analysis for all the simulation results obtained from the QMC sampling.

Fig. 5(b), (e) and (h) exhibits the variations of total recovery volume with time. As expected, the total volumes recovered from the skimmer well are obviously less than those from water- and vacuum-pumping schemes (Fig. 5(b)). According to Fig. 5(e), water pumping would withdraw about 17.7–53.3 m^3 free products with a chance of 95%. In comparison (Fig. 5(h)), the free product withdrawal would be slightly decreased by 1 m^3 approximately by vacuum pumping. This indicates that water pumping would be slightly better than vacuum pumping (if remediation cost was not considered).

As shown in Fig. 5(c), the recovery rate is extremely low, with the upper bound less than 0.015 m^3/day. This means the nature recovery would not be an effective scheme. The water pumping would have the largest recovery rate, with the average rate decreasing from 0.65 to almost zero after about 5 years (less than 0.1 m^3/day) (Fig. 5(f)). The recovery rate of the vacuum pumping would be approximately 77% lower than water pumping at the initial pumping stage; it would also decrease to zero after about 73-day operation (less than 0.1 m^3/day) (Fig. 5(i)). Note that the recovery rates of the three pumping strategies would decrease

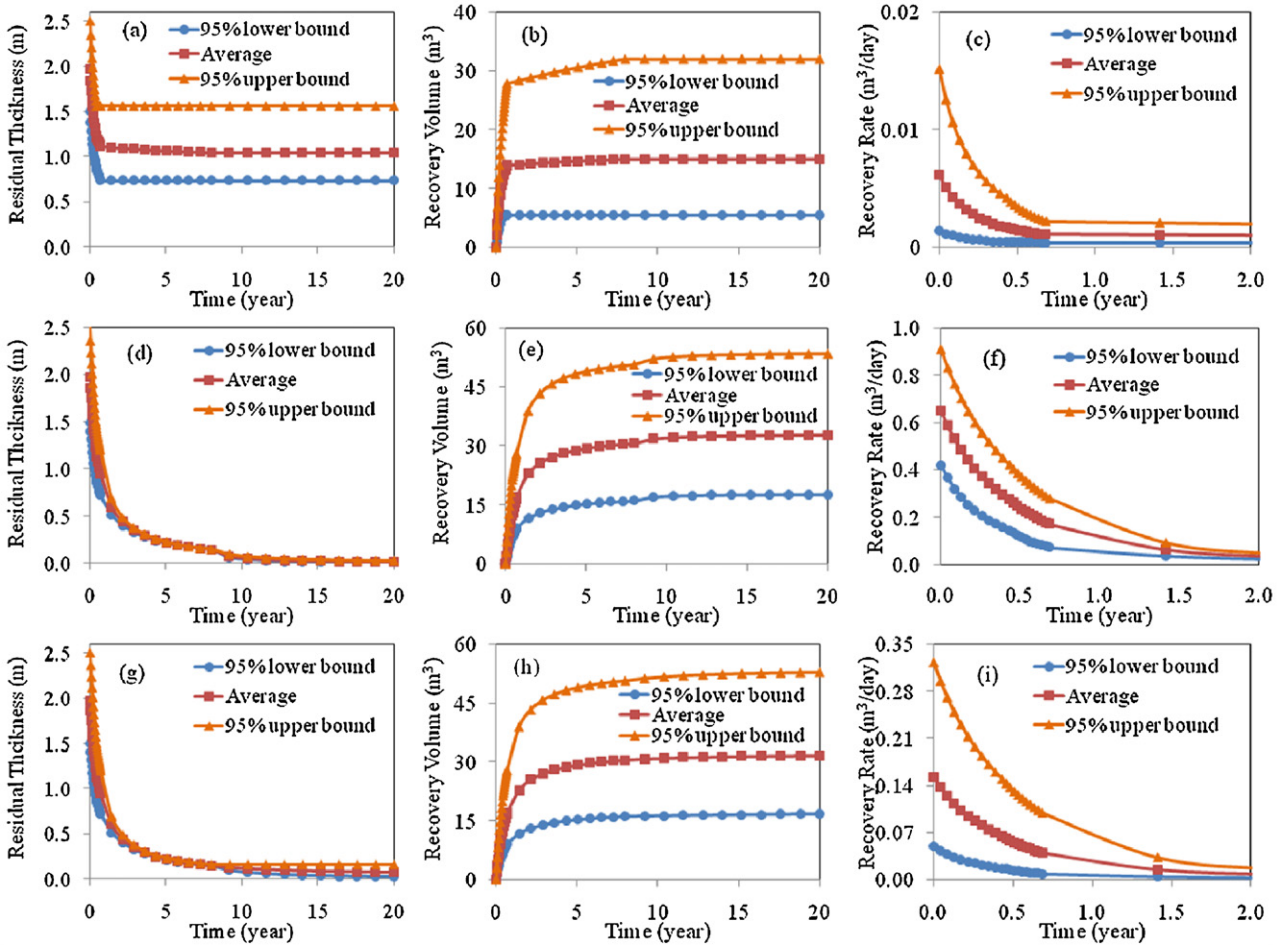

Fig. 5. Free product recovery performance versus time, where (a)–(c) stand for skimmer operation, (d)–(f) stands for water pumping, and (g)–(i) stands for vacuum pumping.

after 2 years (less than 0.05 m^3/day). This implies that a short-term pumping scheme would not be suggested due to its sharp decline in recovery rates. A feasible way to enhance recover efficiency is to introduce multistage pumping [3] or process control strategies [34].

It should be mentioned that this comparison was conducted under the operating conditions of 1 m^3/h for water pumping and −4 m H_2O column for vacuum pumping. It was expected that variation of operation conditions may influence recovery performance. Such an impact and optimization of pumping conditions would be investigated in further studies. Also, different likelihood measures may affect the quality of simulation (good or poor) throughout the entire parameter ranges. Beven and Binley [19] investigated the effect of different likelihood measures on the fit to the daily discharges for the Ringelbach catchment; they found that the effect would be significant, as different measures produced different (narrower or wider) confidence limits in the predictions. Similarly, variation of likelihood measures may also lead to the change of migration and recovery of free products in the aquifer. Moreover, the ranges of the uncertain parameters were determined according to the existing site characterization results. However, it was expected that the actual ranges could be larger than the ones used in this study; this could lead to underestimation of uncertainty predictions of the migration and recovery processes.

4. Conclusions and discussion

A GUSA framework was proposed based on GSA and GLUE methods. Compared to GLUE, GUSA can not only evaluate global sensitivity and uncertainty of modeling parameter sets, but also quantify the uncertainty in modeling predictions. QMC sampling technique was also employed for obtaining realizations of uncertain parameter sets. It has the advantage over traditional MC and LHC in mitigating computational effort. GUSA was applied to a practical petroleum-contaminated site in Canada. Results from GSA showed that (1) initial free product thickness has the most significant impact on total recovery volume but least impact on residual free product thickness and recovery rate; (2) total recovery volume and recovery rate are sensitive to residual LNAPL phase saturations and soil porosity. Results from uncertainty predictions revealed that (1) the residual thickness would remain high and almost unchanged after about half-year of skimmer-well scheme; (2) the rather high residual thickness indicates that natural attenuation would not be suitable for the aquifer remediation. The largest total recovery volume would be from water pumping, followed by vacuum pumping, and then skimmer.

A major feature of QMC is also discussed. Compared to LH sampling, it is convenient to construct a set of samples $x_1, x_2, \ldots, x_N$ in such a way that if the $(N+1)$th sample should be added, the previous N elements need not be recomputed. The LH sampling rule uses samples set with low discrepancy, but requires re-computation (or re-sampling) if N is increased [35]. In addition, LH sampling is not recommended when solving high-dimensional problems where computational effort is intensive. In MC, no re-sampling is needed if N is increased, but there is no guarantee that the samples are of low discrepancy. Therefore, QMC has a desirable feature over the other two methods. More recently, MCMC has shown satisfactory performance in uncertainty estimations [36–38]. However, one challenge associated with MCMC is computational efficiency due to iterative sampling is required; moreover, MCMC is on a basis of a given assumption that the probabilistic density function of a stochastic variable is known. As a result, it may not be suitable for solving problems where probability density functions of outputs are not needed (e.g., use GLUE for calibration and uncertainty estimation of models). One limitation of the proposed framework lies in that it is not suitable for problems with considerably high dimensions owing to QMC's drawback. However, this can be resolved by using mixed QMC and MCMC method if needed. The other issue is regarding the heterogeneity of the aquifer, which may have impact on the global sensitivity and uncertainty predictions. This would be investigated in the extended studies.

Acknowledgments

This research was supported by the Program for New Century Excellent Talents in University of China (NCET-11-0632), the Fundamental Research Funds for the Central Universities, and the Program for Innovative Research Team in University (IRT1127). The authors would like to thank the editor and the anonymous reviewers for their helpful comments and suggestions.

Appendix A. Supplementary data

Supplementary data associated with this article can be found, in the online version, at doi:10.1016/j.jhazmat.2012.03.067.

References

[1] J.J. Kaluarachchi, J.C. Parker, Multiphase flow with a simplified model for oil entrapment, Transport Porous Med. 7 (1) (1992) 1–14.
[2] J.C. Parker, J.L. Zhu, T.G. Johnson, V.J. Kremesec, E.L. Hockman, Modeling free product migration and recovery at hydrocarbon spill sites, Ground Water 32 (1) (1994) 119–128.
[3] J.J. Kaluarachchi, Effect of subsurface heterogeneity on free-product recovery from unconfined aquifers, J. Contam. Hydrol. 22 (3–4) (1996) 19–37.
[4] J.F. Campagnolo, A. Akgerman, Modeling of soil vapor extraction (SVE) systems. II. Biodegradation aspects of soil vapor extraction, Waste Manage. 15 (5–6) (1995) 391–398.
[5] A.A. Jennings, P. Patil, Feasibility modeling of passive soil vapor extraction, J. Environ. Eng. Sci. 1 (2002) 157–172.
[6] P.G. Mihopoulos, M.T. Suidan, G.D. Sayles, S. Kaskassian, Numerical modeling of oxygen exclusion experiments of anaerobic bioventing, J. Contam. Hydrol. 58 (2002) 209–220.
[7] R.J. Charbeneau, R.T. Johns, L.W. Lake, M.J. McAdams, Free-product recovery of petroleum hydrocarbon liquids, Ground Water Monit. Remediation 20 (2000) 147–168.
[8] J.B. Li, G.H. Huang, A. Chakma, G.M. Zeng, Numerical simulation of dual phase vacuum extraction to remove non-aqueous phase liquids in subsurface, ASCE-Practice Periodical Hazard. Toxic Radioactive Waste Manage. 7 (2) (2003) 106–113.
[9] H.K. Yen, N.B. Chang, Bioslurping model for assessing light hydrocarbon recovery in contaminated unconfined aquifer. II. Optimization analysis, ASCE-Practice Periodical Hazard. Toxic Radioactive Waste Manage. 7 (2003) 131–138.
[10] C.L. Weber, J.M. VanBriesen, M.J. Small, A stochastic regression approach to analyzing thermodynamic uncertainty in chemical speciation models, Environ. Sci. Technol. 40 (12) (2006) 3872–3878.
[11] L. He, G.H. Huang, H.W. Lu, G.M. Zeng, Optimization of surfactant-enhanced aquifer remediation for a laboratory BTEX system under parameter uncertainty, Environ. Sci. Technol. 42 (6) (2008) 2009–2014.
[12] L. He, G.H. Huang, H.W. Lu, Health-risk-based groundwater remediation system optimization through clusterwise linear regression, Environ. Sci. Technol. 42 (24) (2008) 9237–9243.
[13] L. He, G.H. Huang, H.W. Lu, Characterization of petroleum-hydrocarbons fate and transport in homogeneous and heterogeneous aquifers using a generalized uncertainty estimation method, ASCE-J. Environ. Eng. 137 (1) (2011) 1–8.
[14] H. Niederreiter, Random Number Generation and Quasi-Monte Carlo Methods, Society for Industrial and Applied Mathematics, 1992.
[15] H.I. Essaid, K.M. Hess, Monte Carlo simulations of multiphase flow incorporating spatial variability of hydraulic properties, Ground Water 31 (1) (1992) 123–134.
[16] A. Montanari, Large sample behaviours of the generalized likelihood uncertainty estimation (GLUE) is assessing the uncertainty of rainfall-runoff simulations, Water Resour. Res. 41 (2005) W08406, http://dx.doi.org/10.1029/2004WR003826.
[17] K.J. Beven, A. Binley, The future of distributed models: model calibration and uncertainty prediction, Hydrol. Process. 6 (1992) 279–2978.
[18] A.P. Jacquin, A.Y. Shamseldin, Development of a possibilistic method for the evaluation of predictive uncertainty in rainfall-runoff modeling, Water Resour. Res. 43 (2007) W04425, http://dx.doi.org/10.1029/2006WR005072.
[19] J. Freer, K.J. Beven, Bayesian estimation of uncertainty in runoff prediction and the value of data: an application of the GLUE approach, Water Resour. Res. 32 (1996) 2161–2173.
[20] S.W. Franks, P. Gineste, K.J. Beven, P. Merot, On constraining the predictions of a distributed model: the incorporation of fuzzy estimates of saturated areas into the calibration processes, Water Resour. Res. 34 (1998) 787–797.

[21] K. Beven, J. Freer, Equifinality, data assimilation, and uncertainty estimation in mechanistic modeling of complex environmental systems using the GLUE methodology, J. Hydrol. 249 (2001) (2001) 11–29.
[22] J.R. Stedinger, R.M. Vogel, S.U. Lee, R. Batchelder, Appraisal of the generalized likelihood uncertainty estimation (GLUE) method, Water Resour. Res. 44 (2008) W00B06, http://dx.doi.org/10.1029/2008WR006822.
[23] G. Freni, G. Mannina, G. Viviani, Uncertainty in urban stormwater quality modelling: the effect of acceptability threshold in the GLUE methodology, Water Res. 42 (8–9) (2008) 2061–2072.
[24] K.J. Beven, Towards integrated environmental models of everywhere: uncertainty, data and modelling as a learning process, Hydrol. Earth Syst. Sci. 11 (1) (2007) 460–467.
[25] P. Mantovan, E. Todini, Hydrological forecasting uncertainty assessment: incoherence of the GLUE methodology, J. Hydrol. 330 (1–2) (2006) 368–381.
[26] R.S. Blasone, J.A. Vrugt, H. Madsen, D. Rosbjerg, B.A. Robinson, G.A. Zyvoloski, Generalized likelihood uncertainty estimation (GLUE) using adaptive Markov Chain Monte Carlo sampling, Adv. Water Resour. 31 (2008) 630–648.
[27] J. Pan, R. Thompson, Quasi-Monte Carlo estimation in generalized linear mixed models, Comput. Stat. Data Anal. 51 (2007) 5765–5775.
[28] DAEM (Draper Aden Environmental Modeling Inc.), MOVER Multiphase Organic Vacuum Enhanced Recovery Simulator: Technical Documentation & User Guide, Draper Aden Environmental Modeling Inc., Blacksburg, VA, 1997.
[29] W.J. Morokoff, R.E. Caflisch, Quasi-Monte Carlo integration, J. Comput. Phys. 122 (2) (1995) 218–230.
[30] L.M. Sobol, Global sensitivity indices for nonlinear mathematical models and their Monte Carlo estimates, Math. Comput. Simul. 55 (2001) 271–280.
[31] G.J. Klir, T.A. Folger, Fuzzy sets, uncertainty, and information, Prentice-Hall, Englewood Cliffs, N.J., 1988.
[32] L. Kocis, W. Whiten, Computational investigations of low-discrepancy sequences, ACM T. Math. Softw. 23 (2) (1997) 266–294.
[33] University of Regina, Numerical simulation, risk assessment, site remediation, and monitoring design – a study of soil and groundwater contamination at the Cantuar field scrubber site, Prepared for TransGas, Regina, Sask., Canada, 2003.
[34] Y.F. Huang, G.Q. Wang, G.H. Huang, H.N. Xiao, A. Chakma, IPCS: an integrated process control system for enhanced in situ bioremediation, Environ. Pollut. 151 (3) (2008) 460–468.
[35] A. Ramaswami, J.B. Milford, M.J. Small, Integrated environmental modeling – pollutant transport, in: Fate and Risk in the Environment, John Wiley & Sons Inc., 2005.
[36] S.A. Miller, A.E. Landis, T. Theis, Use of Monte Carlo analysis to characterize nitrogen fluxes in agriecosystems, Environ. Sci. Technol. 40 (7) (2006) 2324–2332.
[37] A. Hassan, H.M. Bekhit, J.B. Chapman, Using Markov Chain Mote Carlo to quantify parameter uncertainty and its effect on predictions of a groundwater flow model, Environ. Modell. Softw. 24 (6) (2009) 749–763.
[38] T.M. Saloranta, J.M. Armitage, H. Haario, K. Naes, I.T. Cousins, D.N. Barton, Modeling the effects and uncertainties of contaminated sediment remediation scenarios in a Norwegian Fjord by Markov Chain Monte Carlo simulation, Environ. Sci. Technol. 42 (1) (2008) 200–206.